catalysts

MDPI

Article

Abatement of 1,2,4-Trichlorobencene by Wet Peroxide Oxidation Catalysed by Goethite and Enhanced by Visible LED Light at Neutral pH

David Lorenzo [1,*], Aurora Santos [1], Andrés Sánchez-Yepes [1], Leandro Óscar Conte [1,2] and Carmen María Domínguez [1]

[1] Chemical Engineering and Materials Department, Facultad de Ciencias Químicas, Universidad Complutense de Madrid, Ciudad Universitaria S/N, 28040 Madrid, Spain; aursan@quim.ucm.es (A.S.); andsan28@ucm.es (A.S.-Y.); lconte@ucm.es (L.Ó.C.); carmdomi@ucm.es (C.M.D.)

[2] Instituto de Desarrollo Tecnológico para la Industria Química (INTEC), Consejo Nacional de Investigaciones Científicas y Técnicas (CONICET) and Universidad Nacional del Litoral (UNL), Ruta Nacional N° 168, 3000 Santa Fe, Argentina

* Correspondence: dlorenzo@quim.ucm.es; Tel.: +34-913944106

Abstract: There is significant environmental concern about chlorinated organic compounds (COCs) in wastewater, surface water, and groundwater due to their low biodegradability and high persistence. In this work, 1,2,4-trichlorobenzene (124-TCB) was selected as a model compound to study its abatement using wet peroxide oxidation at neutral pH with goethite as a heterogeneous catalyst, which was enhanced with visible monochromatic light-emitting diode (LED) light (470 nm). A systematic study of the main operating variables (oxidant and catalyst concentration and irradiance) was accomplished to investigate their influence in the abatement of 124-TCB in water. The reaction was carried out in a well-mixed reactor of glass irradiated by a visible LED light. The hydrogen peroxide concentration was tested from 0 to 18 mM, the goethite concentration within the range 0.1–1.0 $g{\cdot}L^{-1}$ and the irradiance from 0.10 to 0.24 $W{\cdot}cm^{-2}$ at neutral pH. It was found that this oxidation method is a very efficient technique to abate 124-TCB, reaching a pollutant conversion of 0.9 when using 0.1 $g{\cdot}L^{-1}$ of goethite, 18 mM of H_2O_2, and 0.24 of $W{\cdot}cm^{-2}$. Moreover, the system performance was evaluated using the photonic efficiency (ratio of the moles of 124-TCB abated and the moles of photons arriving at the reactor window). The maximum photonic efficiencies were obtained using the lowest lamp powers and moderate to high catalyst loads.

Keywords: wet oxidation; goethite; LED light; 1,2,4-trichlorobencene; CWPO

Citation: Lorenzo, D.; Santos, A.; Sánchez-Yepes, A.; Conte, L.Ó.; Domínguez, C.M. Abatement of 1,2,4-Trichlorobencene by Wet Peroxide Oxidation Catalysed by Goethite and Enhanced by Visible LED Light at Neutral pH. *Catalysts* **2021**, *11*, 139. https://doi.org/10.3390/catal11010139

Received: 25 December 2020
Accepted: 16 January 2021
Published: 19 January 2021

1. Introduction

The presence of chlorinated organic compounds (COCs) in wastewater, surface water, and groundwater is a significant environmental issue. In accordance to the EU Water Framework Directive (Directive 2000/60/EC), several COCs have been added in the last two decades to the list of substances to be monitored, encouraging limiting their production and use. This list comprises pollutants as 1,1,1-trichloroethane, 1,1,2-trichloroethane, 1,2-dichlorobenzene, 1,2-dichloroethane, 1,4-dichlorobenzene, 2-chlorophenol, 3-chlorophenol, 4-chlorophenol, carbon tetrachloride, chlorine, chlorobenzene, pentachlorobenzene, chloroform, dichloromethane, dioxins and furans, hexachlorobenzene, hexachlorobutadiene, hexachlorocyclohexane, pentachlorophenol, tetrachloroethylene, trichlorobenzene, trichloroethylene, and vinyl chloride [1]. However, due to their extensive use as wood preservatives, pesticide precursors, solvents, hydraulic fluids, dielectric oil, dyes, and other materials [2–7], these COCs still pose a risk for the water quality.

Given the low biodegradability and high persistence of these compounds, several chemical technologies have been proposed for their abatement, including advanced oxidation processes (AOPs) [8]. Among the oxidants, the use of hydrogen peroxide is noteworthy.

To increase the oxidising potential of H_2O_2, this oxidant must be activated to produce radical species able to degrade recalcitrant compounds such as chlorobenzenes. Hydrogen peroxide activation by UV [9,10], UV and ozone [11], soluble iron (Fenton reaction) [12–14], iron nanoparticles (Fenton-like reaction) [15], and power (electro Fenton) [16] has been reported in the literature for the abatement of chlorobenzenes. Despite their effectiveness, several drawbacks remain, such as the high cost associated, the need to operate at acidic pH, and the generation of iron in solution, which must be removed in additional treatments (for example, the neutralisation, separation, and management of the iron hydroxide sludge generated) [17–20]. All of this has encouraged the research for new processes, such as the heterogeneous Fenton process, which is also known as catalytic wet peroxide oxidation (CWPO), in which a solid catalyst is used. CWPO looks for solid catalyst features with negligible leaching of the active phase (iron), environment-friendly materials, and easily separable from the solution [20]. Several attempts have been made to develop solid supports for the active iron species. Unfortunately, this sort of catalyst usually undergoes iron leaching, and the Fenton reaction takes place with homogeneous catalyst instead of solid catalyst. Recently, naturally occurring iron minerals, abundant and cheap materials [21], have been proposed as alternative iron sources in CWPO in the abatement of phenol [17,22] and in the treatment of wastewater [23,24]. In the oxidation of chlorobenzenes, hematite has been successfully applied with hydrogen peroxide [25]. Iron materials are stable and resistant to iron leaching [20,26,27], which is a significant advantage over other synthesised catalysts. The main drawback of these heterogeneous catalysts is the lower rate of H_2O_2 decomposition and, therefore, hydroxyl radical (•OH) generation vs. the classical Fenton process. This fact leads to longer reaction times and restricts their full-scale applications [18,28].

Reducing agents in the reaction medium accelerate the catalytic cycle of iron and thus improve the hydroxyl radicals generation rate. In this way, it was found that hydroxylamine (HA) enhanced the redox cycle of the iron contained in goethite when this mineral was used to abate organic pollutants by CWPO [18]. The addition of HA has also been successfully tested in chlorobenzenes abatement by hydrogen peroxide and goethite [29]. This material was stable, and no iron leaching was found despite the acid pH used (acid pH was required for oxidising the chlorobenzenes) [29]. However, although this reducing agent greatly increases the efficiency of the process, the addition of HA to the reaction system introduces an additional cost and risk to the environment, so other options should be explored.

Alternatively, light as a non-expensive energy source has also been used to enhance the redox cycle of iron in Fenton reaction and the CWPO process. UV light has been wildly applied, but this kind of radiation only represents 4–5% of the solar light, whereas the visible light is about 45% of the solar energy. In this way, many photo-Fenton process applications have been designed with artificial visible light sources such as Hg or Xe lamps. However, these lamps need a complicated cooling system. In addition, they are toxic, energy consuming, and expensive when using in real applications [30]. Commercial visible light-emitting diode lamps (VIS LED) have been utilised as an innovative and efficient light source [30].

Although the homogenous photo-Fenton process has been investigated in the abatement of different contaminants [31], such as pesticides [30,32,33], insecticides [34], and chlorophenols [35], this process presents the same drawbacks as the conventional Fenton [17–20,31]. For these reasons, the use of naturally occurring iron materials (as catalysts) activated by VIS LED to accelerate the iron redox cycle is especially interesting. Goethite is a cheap material, one of the most chemically stable iron oxides, showing excellent results in the process, acting as a visible-light photocatalyst with a bandgap of 2.502 eV [36,37].

Ortiz de la Plata et al. [38,39] have successfully applied the photo-Fenton process for the abatement of 2-chlorophenol using goethite activated by UV-light (350–400 nm) as a catalyst at neutral pH, and they proposed a kinetic model [38]. Mameri et al. studied the heterogeneous photo-degradation of paracetamol (PC) [40] and amoxicillin [41] using goethite as a catalyst. Goethite (1 $g \cdot L^{-1}$) was studied in aqueous suspension without pH

adjustment and irradiated at 365 nm and solar light, with a hydrogen peroxide concentration of 5 mM. These authors reported a higher removal of contaminant using solar radiation due to the higher generation of hydroxyl radicals under this radiation [40,41].

In the current work, goethite activated by light (monochromatic LED light at 470 ± 10 nm) has been used in the CWPO of 1,2,4-trichlorobenzene (124-TCB), which was selected as a model pollutant. This COC is a semi-volatile compound with relatively high water solubility and therefore, it is easily transported in the environment. Due to its toxicity and persistence, this pollutant represents a risk for human health and environmental safety [2,4,6,42]. Thus, it is a pollutant that is highly used as a model compound in other works in literature [43]. To our knowledge, there is a lack of information in the literature concerning the application of LED VIS-light to activate goethite for COCs removal. In this work, LED VIS-light coupled with a naturally occurring iron material was effectively used to abate 124-TCB under neutral pH conditions, solving the main drawbacks of classical Fenton and CWPO.

2. Results

The effect of the main operating variables (oxidant and catalyst concentration and irradiance) in the conversion of 124-TCB, as expressed in Equation (1), has been investigated.

$$X_j = 1 - C_j/C_{j,0} \quad (1)$$

being C_j and $C_{j,0}$ the concentration of j compound (124-TCB or H_2O_2) at different reaction times and the initial concentration of these compounds, respectively, in $mg \cdot L^{-1}$.

The experimental conditions of runs carried out to study the influence of variables in the 124-TCB abatement are summarised in Table S1 of the Supplementary Material. In these runs, pH was neutral, and the temperature of the reaction mixture was kept at 25 °C. Experiments B1–B5 refer to blank experiments in which the value of a variable was set to zero.

As can be seen in Table S1, run B1 was carried out in the absence of catalyst and oxidant to study the effect of light on 124-TCB concentration. At the conditions tested, a negligible change in pollutant concentration was noticed with time. Therefore, neither pollutant conversion nor evaporation took place in this run in the time period studied (6 h).

2.1. Effect of Peroxide Hydrogen Concentration

In experiment B2, the consumption of hydrogen peroxide in the presence of goethite (0.5 $g \cdot L^{-1}$) activated by LED light was studied. The reaction was carried out without 124-TCB, and the hydrogen peroxide concentration was monitored over time. It was found that the conversion of hydrogen peroxide was negligible after 6 h of reaction. Thus, in the absence of 124-TCB, the consumption of oxidant is insignificant.

The effect of hydrogen peroxide concentration in the degradation of 124-TCB in water was studied in runs R1–R3 and B3 (Table S1, experiment carried out in the absence of the oxidant). The oxidant dose used varied from 0 to 10 times the stoichiometric amount, which was calculated assuming the complete mineralisation of the initial concentration of 124-TCB. The total mineralisation reaction is summarised in Equation (2).

$$C_6H_3Cl_3 \text{ (124-TCB)} + 12\ H_2O_2 \rightarrow 6\ CO_2 + 3\ HCl + 12\ H_2O \quad (2)$$

Figure 1 shows the conversion of 124-TCB achieved at different reaction times, using the same concentration of goethite and irradiance while using different initial hydrogen peroxide concentrations. As is shown, at 360 min, the highest pollutant conversion value ($X_{124,TCB}$ = 0.89) was achieved using ten times the stoichiometric amount of oxidant (C_{H2O2} = 18.1 mM). Small differences were found utilising a half dosage (C_{H2O2} = 9.1 mM) but $X_{124,TCB}$ dropped to 0.75 when the stoichiometric amount of oxidant was used. This behaviour can be explained attending to the lower production of hydroxyl radicals generated when lower doses of hydrogen peroxide are used. As shown in Figure 1, when hydrogen

peroxide was not added to the reaction mixture (experiment B3), the conversion of 124-TCB is minimal. The latter proved that at the operating conditions tested, the pollutant was removed neither by evaporation nor by adsorption, as noticed in B1, and in agreement with reported elsewhere [29] using goethite as a catalyst but in the absence of light.

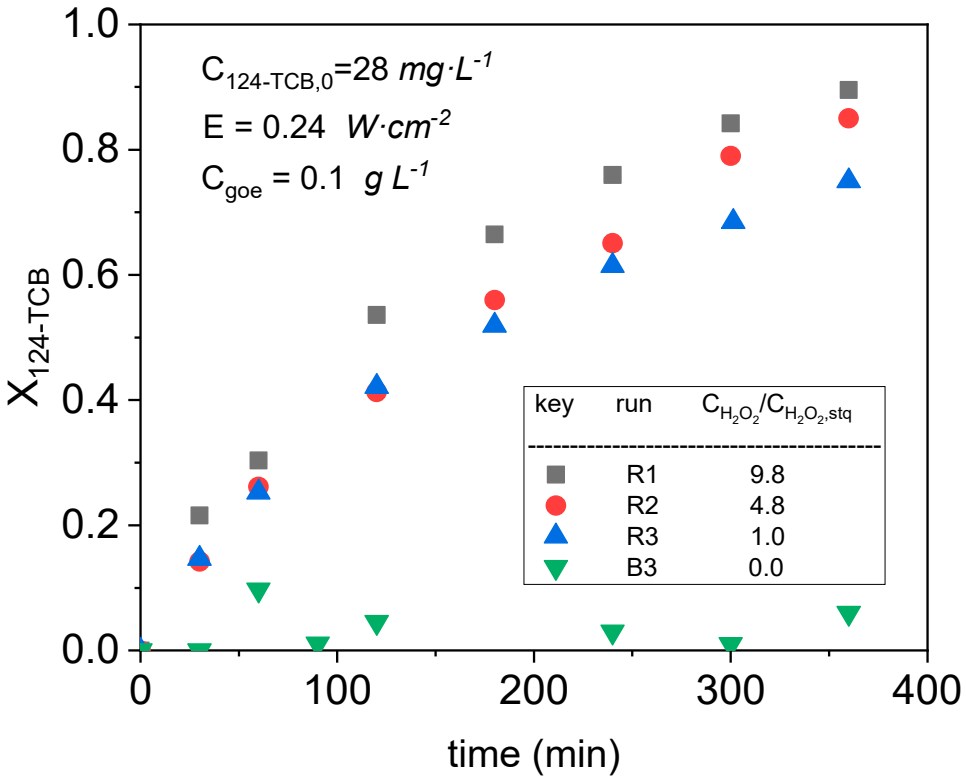

Figure 1. Conversion of 1,2,4-trichlorobenzene (124-TCB) ($X_{124-TCB}$) vs. reaction time at different doses of H_2O_2 at neutral initial pH, C_{GOE} = 0.1 g·L^{-1}, and I = 0.24 W·cm^{-2}, at 25 °C.

Under the conditions studied in Figure 1, the consumption of hydrogen peroxide was monitored. Figure 2 shows that the highest oxidant conversion (X_{H2O2} = 0.15) was found when the lowest stoichiometric ratio was used (run R3). After 360 min of reaction, hydrogen peroxide conversion was lower than 0.10 in runs R2 and R3. The high stoichiometric excess of the oxidant in these runs can explain this low consumption. The pH of the solution was measured at 360 min, finding a value close to 6.5 in all the runs.

2.2. Effect of Goethite Concentration

The goethite concentration effect on 124-TCB removal was investigated in runs R1, R4, R5, R6, and B4 in Table S1. The concentration of goethite was varied within the range 0–1 g·L^{-1}, keeping constant the initial concentration of 124-TCB, amount of oxidant, and irradiate power of the source light.

It was noticed that the addition of the heterogeneous catalyst produced an orange suspension (the higher the concentration of goethite, the higher the color intensity). The conversion of 124-TCB profiles with reaction time for different concentrations of goethite is plotted in Figure 3. It can be seen that when goethite was not added to the reaction media, the conversion of 124-TCB was negligible. This result also proves the negligible evaporation of the pollutant under the operational conditions used, as previously stated.

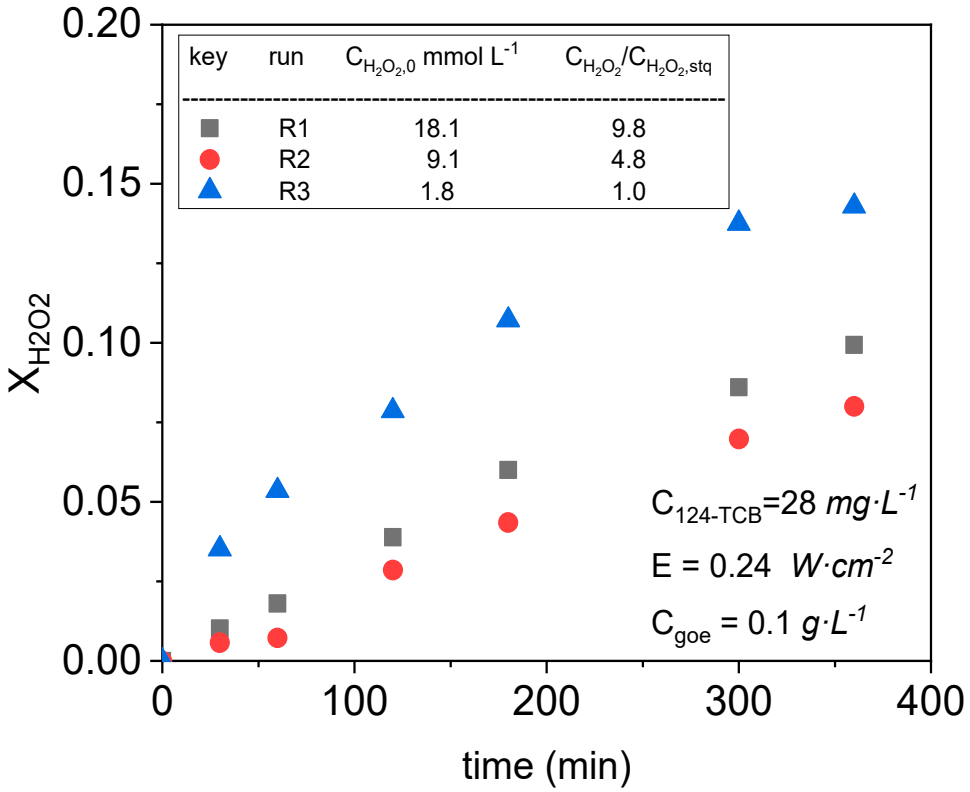

Figure 2. Conversion of hydrogen peroxide (X_{H2O2}) vs. reaction time at different initial doses of H_2O_2. Neutral initial pH, C_{GOE} = 0.1 g·L^{-1}, and I = 0.24 W·cm^{-2}, at 25 °C.

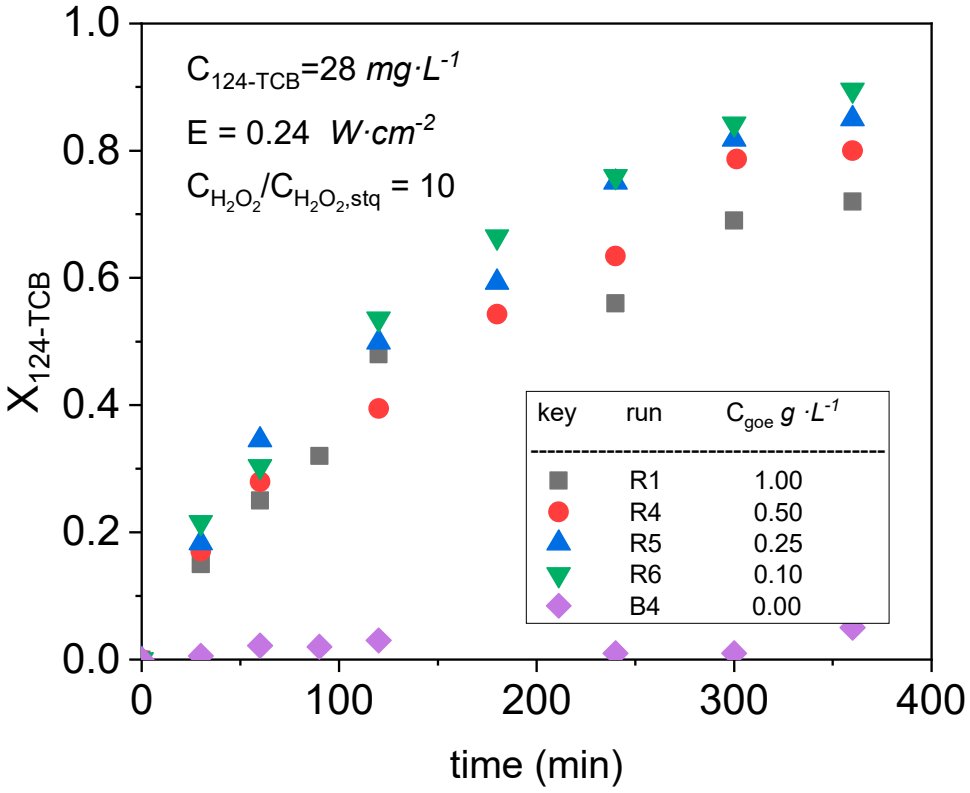

Figure 3. Conversion of 124-TCB vs. reaction time with different concentrations of goethite at neutral initial pH, $\frac{C_{H_2O_2,0}}{C_{H_2O_2,stq}}$ = 10, and E = 0.24 W·cm^{-2}, at 25 °C.

As shown in Figure 4, a drop in the pollutant conversion is noticed when the catalyst concentration increases from 0.10 g·L^{-1}. Smaller differences in the conversion of 124-TCB were found in the goethite concentration range from 0.10 to 0.25 g·L^{-1}. At the final reaction time, 360 min, the conversion of 124-TCB vs. goethite concentration is plotted at the same irradiance and initial oxidant concentration (Figure 4). The higher the concentration of goethite, the lower the obtained conversion of the pollutant.

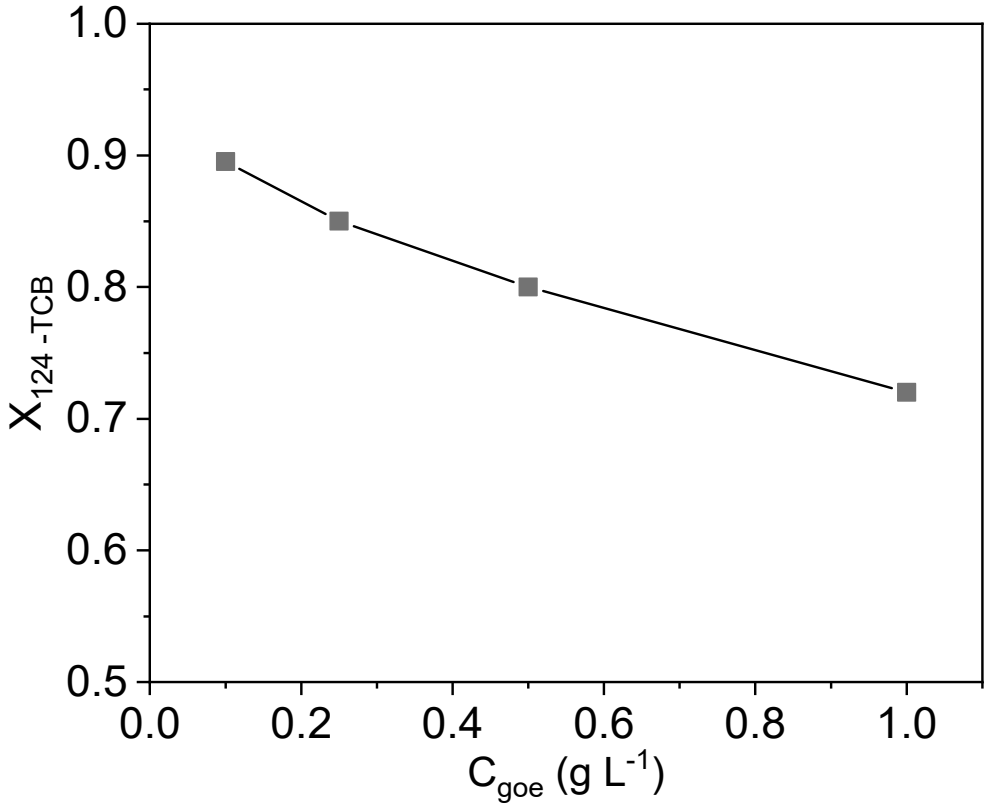

Figure 4. Conversion of 124-TCB vs. goethite concentration at 360 min at neutral initial pH, $\frac{C_{H_2O_2,0}}{C_{H_2O_2,stq}}$ = 10, and I = 0.24 W·cm^{-2}, at 25 °C.

The effect observed in Figure 4 can be explained assuming that the reaction takes place on the solid's surface. The active catalyst surface can be affected by two different phenomena: (i) in a well-mixed reactor, the solid can form agglomerates of the catalyst, which produce a defective liquid–solid contact, meaning a lower conversion of the pollutant than expected [29]; (ii) the oxidation of the pollutant is caused by the hydroxyl radicals produced at the solid surface [44–47]. However, working at a very low catalyst concentration presents operative problems, and therefore, a catalyst concentration of 0.1 g·L^{-1} has been chosen as the optimal value for this study.

Under these conditions, the conversion of 124-TCB was 90% after 6 h of reaction; this value is higher than that obtained in previous work [29] using hydroxylamine and pH = 3 for 124-TCB. In that work, the conversion of 0.7 was obtained at 6 h of reaction but using hydroxylamine (2.5 mmol L^{-1}) and pH = 3 and goethite and a ratio of stoichiometric hydrogen peroxide about 10 (hydroxylamine was not effective at pH = 7). Barbash et al. studied the abatement of 124-TCB using persulfate and thiosulfate in river sediments; they found a conversion of 75% after 5 h of reaction [48]. Similarly, Liu et al. reported a conversion close to 100% after 1 h of reaction using cabbage-like Co3O4 but using very severe temperature conditions (300 °C) and catalyst concentration [49].

The iron leaching from the solid catalyst to the aqueous phase was studied, measuring the total iron in solution at 360 min of reaction time by atomic emission spectroscopy. The

iron concentration found in all cases was lower than 0.3 mg·L^{-1}. The low content of Fe in the aqueous phase proves that the Fenton-like reaction takes place on the surface of the solid catalyst.

2.3. Effect of Irradiance Used

The effect of absolute irradiance in the abatement of 124-TCB was investigated, varying the nominal power of the LED light source (Figure 5). As can be seen, the conversion of 124-TCB was negligible when the lamp was turned off (run B5). The higher the absolute irradiance applied, the higher the pollutant conversion that was found. As the power increases, the differences decrease. Thus, the difference of 124-TCB conversion achieved between 0.18 and 0.24 W·cm^{-2} was lower than the difference found between 0.10 and 0.18 W·cm^{-2}.

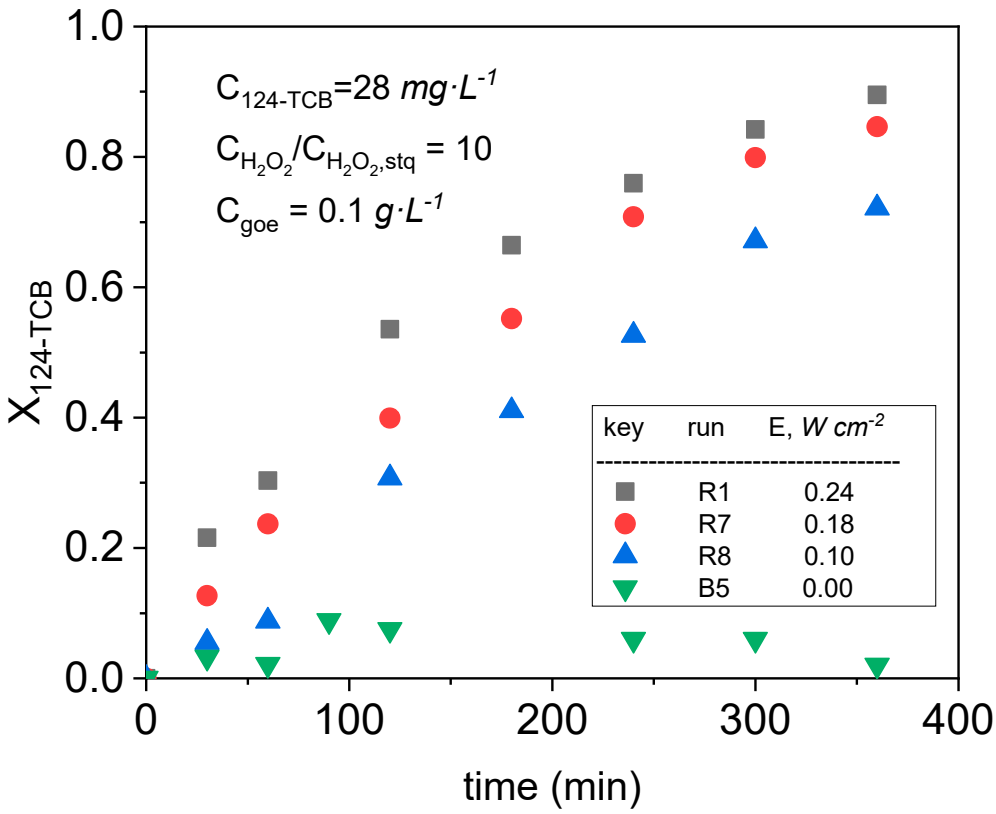

Figure 5. Conversion of 124-TCB vs. reaction time at difference irradiance values at neutral initial pH, $\frac{C_{H_2O_2,0}}{C_{H_2O_2,stq}} = 10$, and $C_{goe} = 0.10$ g·L^{-1}, at 25 °C.

The interaction of LED light and the catalyst surface was studied in runs R4 to R6 and runs R7 to R9. The conversion of 124-TCB was measured at 2 h of reaction time, using the same initial concentration of hydrogen peroxide but varying the goethite concentration and irradiance (Figure 6). As can be seen, at the lowest goethite concentration tested (0.1 g·L^{-1}) and the higher irradiance, the maximum conversion of 124-TCB was obtained. Here, the goethite surface showed more activity in producing hydroxyl radicals because of the increasing number of photons used, which can trigger more electron–holes on its surface [30]. However, using higher concentrations of catalyst, the conversion of the pollutant was not improved. At 0.25 g·L^{-1}, the higher conversion was found between 0.10 and 0.17 W·cm^{-2}, but it was not increased using 0.24 W·cm^{-2}. The agglomeration of the catalyst and the light scattering produced at high catalyst concentration yield a negligible effect of the irradiance in the conversion using 0.5 and 1 g·L^{-1}.

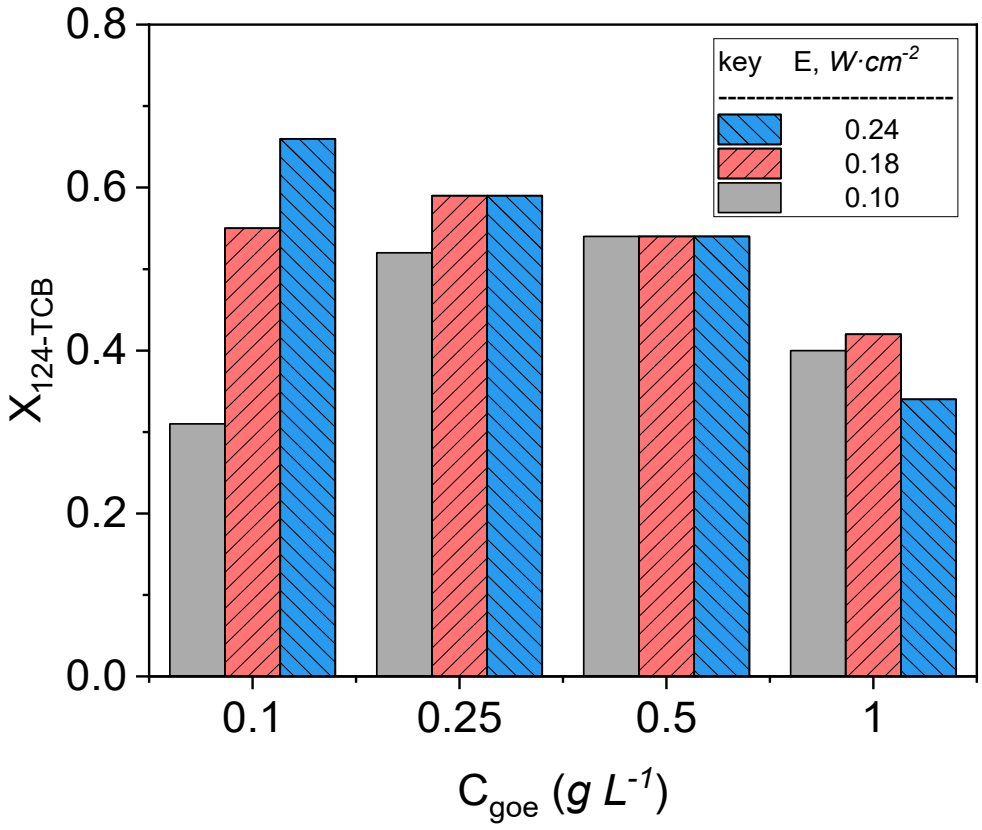

Figure 6. Conversion of 124-TCB vs. goethite concentration at different irradiance values at neutral initial pH, $\frac{C_{H_2O_2,0}}{C_{H_2O_2,stq}} = 10$, and $t = 120$ min, at 25 °C.

To quantify and compare the photo-degradation of 124-TCB under different operating conditions, the photonic efficiency (η_p) was computed (see Equation (3)) [50,51].

$$\eta_p = \frac{C_{124-TCB,0} \cdot X_{124-TCB} \cdot V_R}{F_E \cdot \left(t_f - t_0\right)} \quad (3)$$

being $C_{124-TCB,0}$ and $X_{124-TCB}$ the initial concentration of 124-TCB, in mol·L^{-1}, and 124-TCB conversion, respectively, which was achieved at the time t_f, in s. V_R is the reactor volume (0.1 L), and F_E is the flow of photons, in Einstein s^{-1}, which was irradiated over the reactor window. This photonic efficiency relates the number of moles of pollutant converted after 2 h of reaction with the number of photons arriving at the reactor window over a defined range of wavelengths.

The photons flow in the reactor window (F_E) was estimated using Equation (4). Here, the absolute incident irradiance (I_a) was measured in three different positions over the reactor window.

$$F_E = \int_0^A \int_{\lambda_0}^{\lambda_f} \frac{I_a}{h \cdot \frac{c}{\lambda}} \cdot d\lambda \cdot dA \quad (4)$$

where I_a is the average of absolute irradiance measured with the spectrometer coupled with an optical fiber and a cosine corrector in W·cm^{-2}·nm^{-1}; λ is the wavelength and, h and c are the Plank constant at light speed, respectively. A is the total evaluated area in cm^2.

From the averages values of irradiance plotted in Section 3.2 and integrating in Equations (4) and (3) and using the experimental results of the 124-TCB conversion provided in Figure 6, the photonic efficiency can be calculated for different goethite concentrations and absolute irradiance (please see Table 1).

Table 1. Photonic efficiencies at different catalyst concentration and irradiances, calculated from the experimental values of 124-TCB conversion in Figure 6 and the photons flow irradiated over the reactor window, using Equation (3). The values are summarised in Table S2.

	I, W·cm^{-2}		
C_{goe}, g·L^{-1}	**0.10**	**0.18**	**0.24**
0.1	1.74×10^{-4}	1.74×10^{-4}	1.56×10^{-4}
0.25	2.91×10^{-4}	1.86×10^{-4}	1.39×10^{-4}
0.5	3.03×10^{-4}	1.71×10^{-4}	1.27×10^{-4}

Firstly, the system performance should be noted according to the catalyst load used for each radiation intensity evaluated (please see Table 1). For minimum radiation intensities (I = 0.10 W·m^{-2}), the system photonic yield increases at higher catalyst loads, generating this maximum for 0.5 g·L^{-1} of goethite ($\eta_p = 3.03 \times 10^{-4}$). However, by reducing the catalyst load by 50% (C_{goe} = 0.25 g·L^{-1}), this η_p is only reduced by 4% (2.91×10^{-4} vs. 3.03×10^{-4}). On the other hand, for maximum radiation intensities (I = 0.24 W·m^{-2}), the maximum η_p values are reached for the lowest catalyst concentrations. Here, the scattering out produced by the catalyst particles is a determining factor in the efficiency of the process. Therefore, the knowledge of these photonic efficiencies indicates the energy performance attained with the process and the cost associated with the catalyst load used.

2.4. Oxidation Byproducts and Dechlorination

The concentration of chlorine atoms released by dechlorination of 124-TCB was measured at the final reaction time (360 min) in runs R1 to R12 (experimental conditions summarised in Table S1). The stoichiometric concentration of chloride was calculated using the experimental conversion of the pollutant and Equation (5).

$$C_{Cl^-}^{stc} = C_{124-TCB,0} \cdot X_{124\ -\ TCB} \cdot n \cdot PM_{Cl} \quad (5)$$

where $C_{Cl^-}^{stc}$ is the stoichiometric amount of chloride released to the aqueous phase assuming the complete dechlorination of 124-TCB in mg·L^{-1}; $C_{124\ -\ TCB,0}$ is the initial concentration of the pollutant (0.15 mM) and $X_{124-TCB}$ is the experimental conversion of the contaminant at 360 min of reaction. In addition, n is the number of chlorine released (3, as is shown in Equation (2), and PM_{Cl} is the molar weight of chlorine (35.5 g·mol^{-1}).

Figure 7 shows the experimental and stoichiometric data of chloride concentration measured in runs R1 to R12. As can be seen, the experimental concentration of chloride in the aqueous phase is lower than expected by stoichiometry. Therefore, the total dechlorination of 124-TCB is not reached, forming chlorinated intermediate compounds [52]. These could be unidentified products or volatile chlorinated by-products, which could evaporate from the reaction media. Moreover, the higher conversion of 124-TCB, the lower the difference between these values (experimental and stoichiometric). Thus, the higher conversion of 124-TCB is related to mild oxidant reaction conditions, promoting the fast mineralisation of the chlorinated by-products, avoiding its volatilisation from the reaction media.

To elucidate the by-products of 124-TCB oxidation, the organic compounds generated in an experiment where 18 mg of 124-TCB were added to 100 mL of water, as detailed in the experimental section, were qualitatively analysed. This amount of 124-TCB remains partially non-dissolved at the initial reaction time but disappears with the reaction progress. The solubilised 124-TCB was oxidised, and a new equilibrium was reached between the aqueous and organic phases. Aqueous phase samples were taken at different reaction times, being extracted with n-hexane and analysed by GC-MS. The organic compounds identified in these samples are listed in Scheme 1. The main by-products detected from 124-TCB oxidation are 1,2-dichlorobenzene (12-DCB) and 1,4 dichlorobenzene (14-DCB). Moreover, traces of trichlorophenols (235-TCP and 245-TCP) and chlorobenzene were found (less than 1 mg·L^{-1}). At the beginning of the reaction (30 min), traces of two-ring aromatic chlorinated

compounds were also detected (2,2′,4,4′,5,5′-hexachloro-1,1′-Biphenyl). 235-TCP, 245-TCP, and 2,2′,4,4′,5,5′-hexachloro-1,1′-Biphenyl were identified comparing the mass spectra of each peak in the GC/MS chromatogram with the National Institute of Standards and Technology (NIST) library records [53] (version NIST011) obtaining a match-factors higher than 95%.

At early stages of the reaction, concentrations of 12-DCB and 14-DCB up to 4 $mg \cdot L^{-1}$ were detected, decreasing these concentration values with the reaction progress. These compounds have a lower boiling point (180 °C, and 174 °C, respectively) than 124-TCB (214 °C) and, therefore, they can be more easily removed from the reaction media by volatilisation. Moreover, these compounds can be oxidised at higher rates than 124-TCB [29]. Similarly, CB has a low boiling point (132 °C) and could be easily removed from the aqueous phase by evaporation. The volatilisation of CB and DCBs will explain the mismatch of chlorides in the chlorine mass balance. On the other hand, the higher the oxidation media strength, the higher the by-products oxidation rate and the lower the volatilisation that occurs, explaining the better fit of chloride mass balance at these conditions (Figure 7).

At the final reaction time (360 min), no other chlorinated compounds, apart from those previously stated, were detected by GC/ECD and GC/MSD. Only short-chain organic acids (mainly acetic acid, less than 24 $mg \cdot L^{-1}$) were detected as oxidation by-products at the final reaction time. That means that the treatment studied in the current work leads to the detoxification of the polluted water.

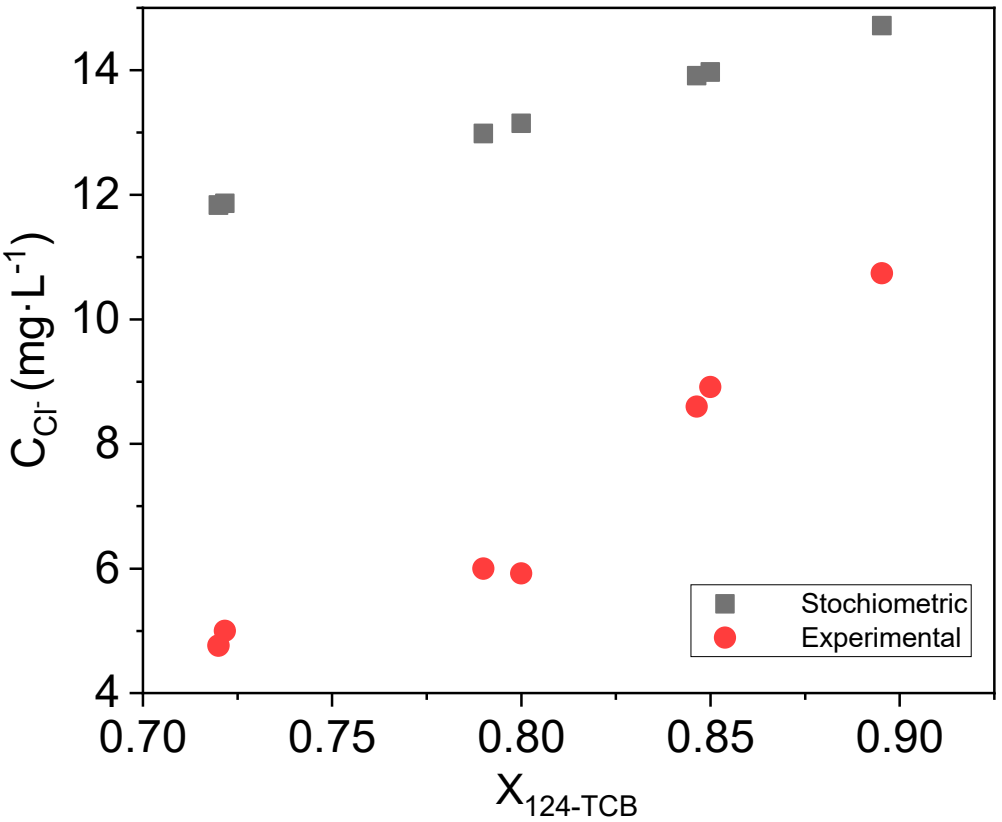

Figure 7. Concentration of chloride generated (experimental) and stoichiometric at the final reaction time (360 min) in the experiments summarised in Table S1.

Compounds identified by GC/MS

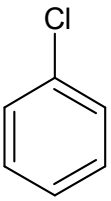

Chlorobencene (traces)

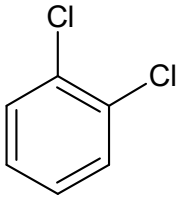

1,2-dichlorobencene (up to 1 mg·L^{-1})

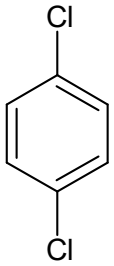

1,4-dichlorobencene (up to 3 mg·L^{-1})

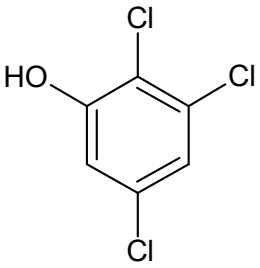

2,3,5-trichlorophenol (traces)

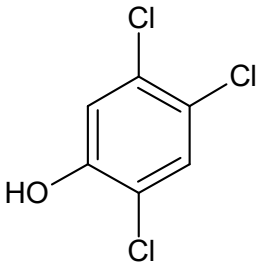

2,4,5-trichlorophenol (traces)

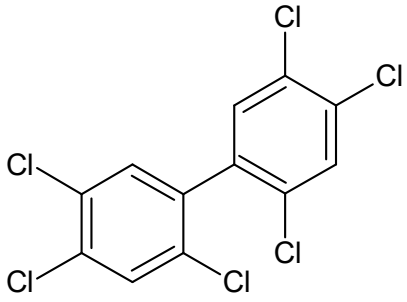

2,2′,4,4′,5,5′-hexachloro-1,1′-Biphenyl (traces)

Scheme 1. Organic by-products found as intermedia in the degradation of 124-TCB using 18 mM of H_2O_2, 0.1 g·L^{-1} of goethite, and 18 mg of pure 124-TCB in 100 mL of water with an absolute irradiance of 0.24 W·cm^2 after 60 min of reaction.

2.5. Catalyst Stability Test

The stability of goethite as a catalyst in CWPO enhanced by visible LED light was tested in cycles of 24 h of reaction, using the highest irradiance value (I = 0.24 W·cm^{-2}), 0.1 g·L^{-1} of goethite concentration (selected previously as an optimal load of catalyst), and 18 mM of H_2O_2. The catalyst recovering from the reaction media was unaffordable due to the low concentration used, and therefore, it was decided to add more 124-TCB to the reaction media at the beginning of each cycle, as explained in the experimental

section. Thus, 18 mg of pure 124-TCB were added to 100 mL of the aqueous phase at the beginning of each new cycle. Five cycles were carried out, each one lasting for 24 h. Hydrogen peroxide was also added at the beginning of each cycle to keep the initial oxidant concentration constant. The oxidant concentration was measured at the end of the cycles. It was found that the consumption of hydrogen peroxide at each cycle was around 20%. The pH at the end of the cycles was also measured, and this value was close to 6.5.

The conversion of 124-TCB at the end of a certain number of cycles was measured. The total reactor content was sacrificed, and n-hexane was added to the reactor content to extract the organic compounds. It was found that the conversion of 124-TCB was almost complete at the end of each cycle. Moreover, no chlorinated by-products were accumulated in the reaction medium. Therefore, it can be concluded that goethite shows a good catalyst activity and high stability, at least at the five reaction cycles tested.

The dechlorination of 124-TCB was studied at the end of each cycle, measuring the chloride concentration in the aqueous phase. Figure 8 shows the stoichiometric concentration of chloride ions (estimated from Equation (2)) and the experimental concentration measured in the aqueous phase. As can be seen, some differences between the theoretical and real values of chlorides concentration were noticed. This fact can be explained due to the formation of the chlorinated by-products previously identified that could be partially volatilised. Remarkably, the chloride mass balance fits better when the number of cycles increased. This finding can be explained considering that DCBs and other chlorinated by-products produced at each cycle are not removed from the media in the successive cycles. Therefore, they have higher reaction rates than 124-TCB to be oxidised, releasing the corresponding chlorides to the aqueous phase.

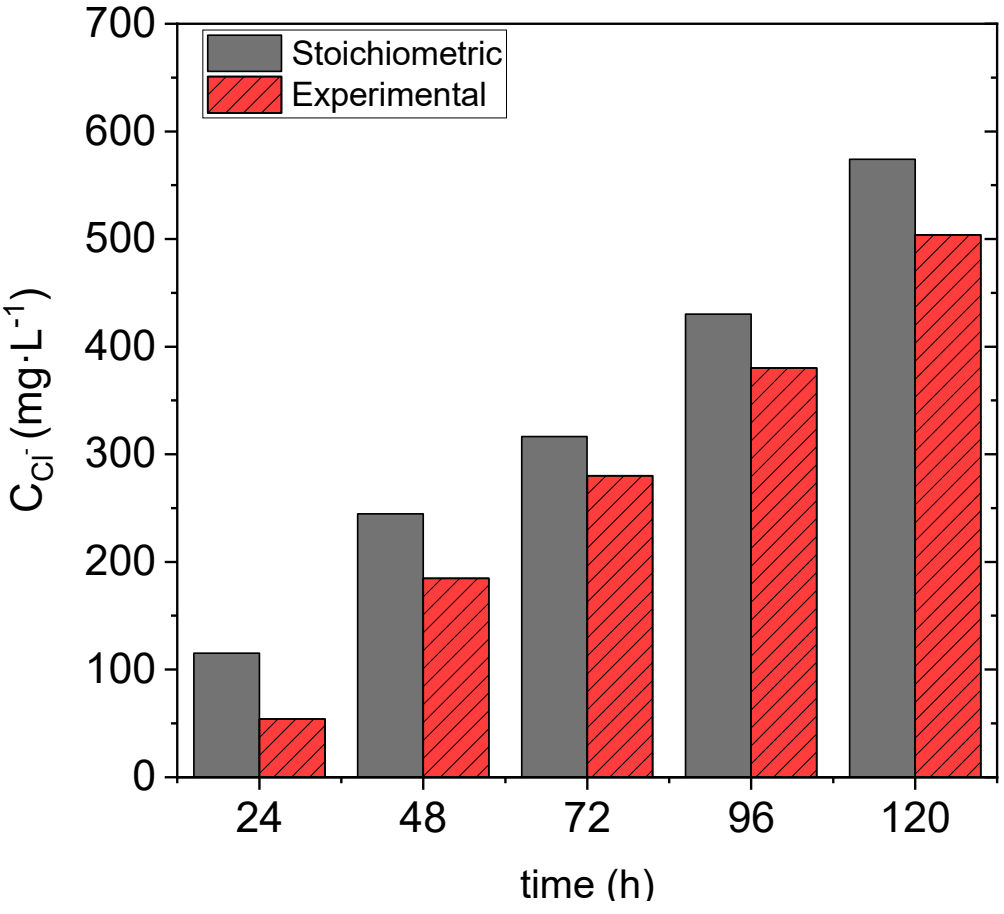

Figure 8. Chloride concentration in the aqueous phase after different times on stream.

Moreover, the high chloride concentration obtained in successive cycles does not decrease the efficiency of the CWPO. Therefore, this catalyst could be applied to real wastewater, surface water, or groundwater that usually show high chlorine content (up to 500 $mg \cdot L^{-1}$). Moreover, after 120 h of reaction, only 1.3 $mg \cdot L^{-1}$ of total iron was found in the aqueous phase. The goethite used shows excellent physicochemical stability in the CWPO process.

3. Materials and Methods

124-TCB, 12-DCB, 14-DCB, and CB of analytical quality were purchased from Sigma-Aldrich (Darmstadt, Germany). Those pure compounds were dissolved in n-hexane (Sigma-Aldrich Darmstadt, Germany) to prepare the standards used in the calibration curves. The quantification of pollutants in reaction samples was accomplished using bicyclohexyl as a standard internal compound (ISTD) purchased from Sigma-Aldrich (Darmstadt, Germany). To simulate the polluted water, 124-TCB was spiked in milli-Q water. The water saturation was carried out under controlled temperature (25 °C ± 1 °C) and 72 h of agitation; the 124-TCB saturation concentration was 28 $mg \cdot L^{-1}$ (0.15 mM).

Hydrogen peroxide (35 wt %), used as oxidant, was supplied by Sigma-Aldrich (Darmstadt, Germany). The theoretical stoichiometric dosage of H_2O_2 required for the total mineralisation of 124-TCB in the saturated water was 63 $mg \cdot L^{-1}$ (1.86 mM). Goethite, used as a catalyst in CWPO reactions, was supplied by Sigma-Aldrich (Darmstadt, Germany). It was compounded by 57.3 wt % of Fe (III), with a specific surface area (S_{BET}) of 10.24 m^2/g [29].

Other reagents used in the present work were used to quantify H_2O_2 (titanium oxisulfate, Sigma-Aldrich (Darmstadt, Germany)) and chloride concentration and short-chain organic acids by Ion Chromatography (sodium carbonate, sodium bicarbonate, sulphuric acid, and acetone, all of them from Sigma-Aldrich Darmstadt, Germany).

3.1. Experimental Setup

The experiments were carried out in a cylindrical batch reactor made of borosilicate glass, with an operating volume of 0.1 *L*. The reaction mixture was well agitated in a magnetic plate, IKA C-MG HS 7 (Staufen, Germany), decreasing the mass transfer limitations. A jacket and a pumping bath of water were used to maintain a constant temperature in the reactor, and the temperature was fixed using a PID controller at 25 °C. The reaction mixture was illuminated with an LED lamp located at the top of the reactor. The distance between the light and the reaction surface was 110 mm. A scheme of the experimental setup is shown in Figure 9. The light source was provided by a High-power collimated LED of Migthtex (LCS-0470-50-11, Lasing, Spain). The LED emits at 470 nm. The LED features an integrated heat sink and a cooling fan.

The light emitter was placed at the focal plane of a collimating lens with a clear aperture of 11 mm (pre-adjusted in the factory). The collimator light sources produce an optical power output of up to 4.17 W. The power could be adjusted using a Mightex BLS-13000-1E LED controller. The output current (0–13 A) can be controlled manually. The light LED source emits over a surface reaction of 11 cm^2 (reactor window).

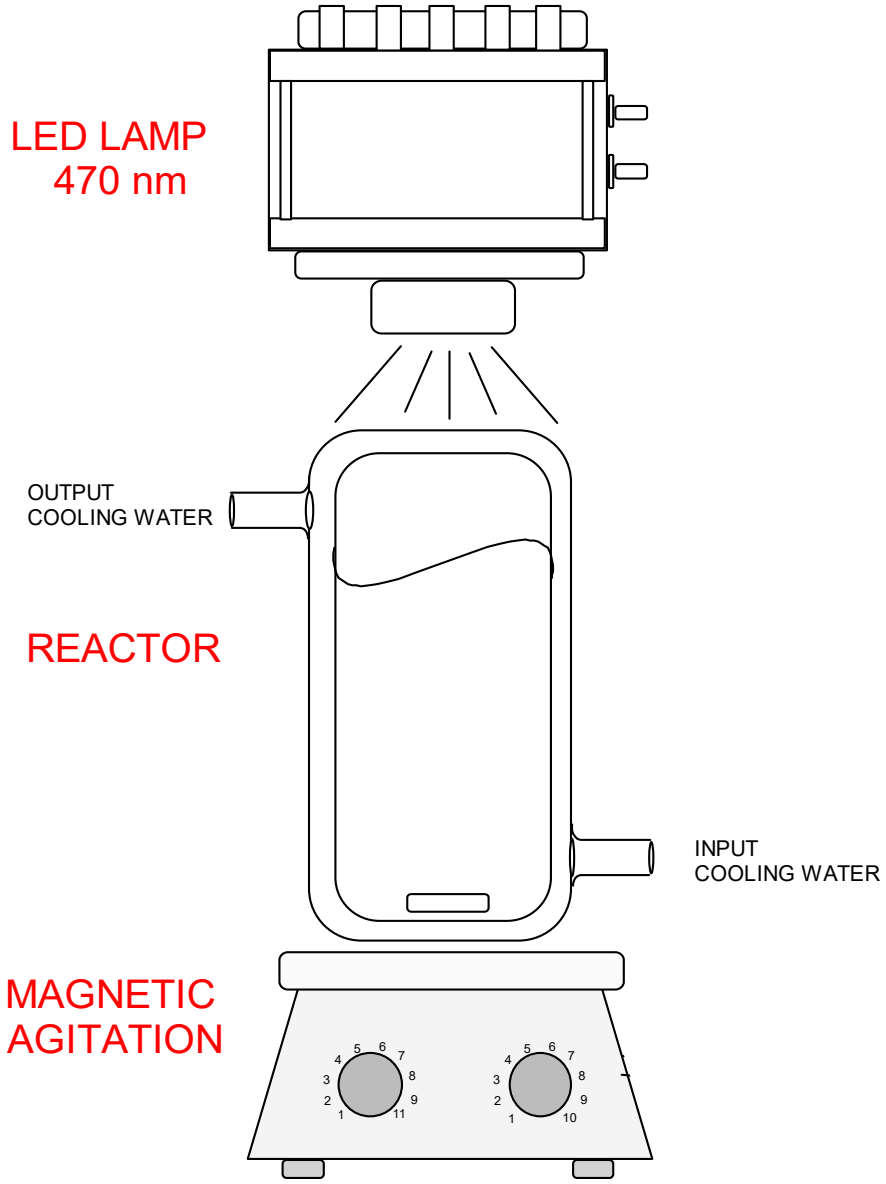

Figure 9. Schematic representation of the experimental setup used.

3.2. Selection of the Wavelength of the LED Light

The role of the LED light in the abatement of 124-TCB is to enhance the redox cycle of Fe (III) to Fe (II) in the Fenton-like reaction. The first step was to select the best wavelength in which goethite presents the lowest transmittance, ensuring the highest absorbance of incident energy by the material. Figure 10a shows the transmittance (T) of goethite at different wavelengths, considering the diffuse reflection to calculate it. The inflection point was located at 545 nm, using the first derivate of the transmittance to wavelength shown in Figure 10b. At this wavelength, a tangential line to the transmittance curve (dotted line in Figure 10a) is plotted. The line cuts the x-axis at 500 nm, so the optimal wavelength, where the lowest transmittance is found (maximum absorbance), is lower than 500. In this way, the wavelength of the lamp source was selected as 470 nm. In this case, photons have the energy ($h\nu$) of 2.6 eV, which is larger than the energy gap (EG) of the goethite (2.2 eV). This conclusion was in concordance with that previously reported in the literature [41].

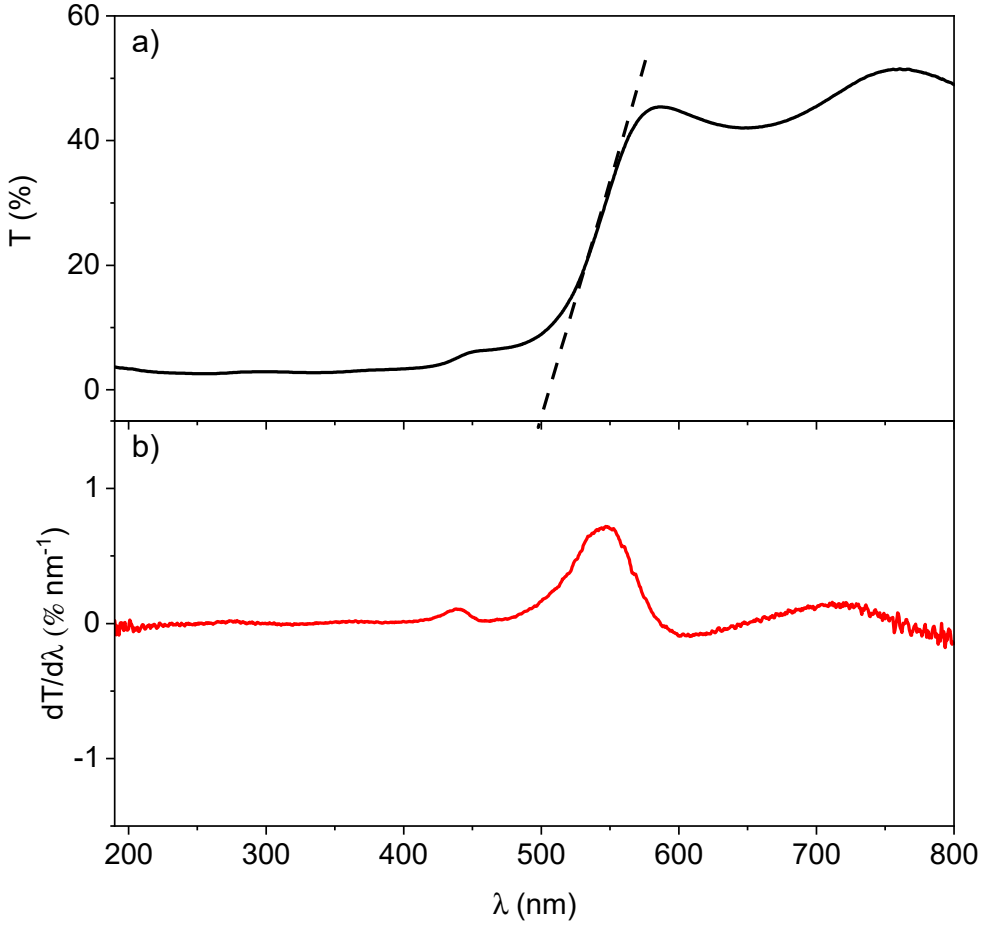

Figure 10. (**a**) Wavelength swapping of transmittance (T) of the surface of goethite. (**b**) First derivate of the transmittance to wavelength.

The absolute irradiance (I) of the LED lamp calculated with Equation (6) was measured over the reactor window (11 cm^2) at different lamp nominal power (Pn) within the range 1.04–4.17 W. Here, a UV-VIS spectrometer coupled with an optical fiber was used.

$$I = \int_{350}^{565} I_{a,\lambda} \cdot d\lambda \quad (6)$$

where I is the total absolute irradiance ($\mu W \cdot cm^{-2}$), and $I_{a,\lambda}$ is the discretised spectral irradiance ($\mu W \cdot cm^{-2} \cdot nm^{-1}$) over the reactor window (11 cm^2) In Figure 11, the values of $I_{a,\lambda}$ for different real lamp nominal power (Pn) over the reactor window (11 cm^2) are given.

Moreover, as can be seen in Table 2, the real lamp power (E) is close to its nominal (Pn) value over the reactor window.

Table 2. Total power irradiated and total irradiance at the surface of the reaction mixture at the reactor window.

	E, W	**I, W·cm^{-2}**
Pn, W	**Top**	**Top**
3.13	2.64	0.24
2.09	1.98	0.18
1.04	1.01	0.10

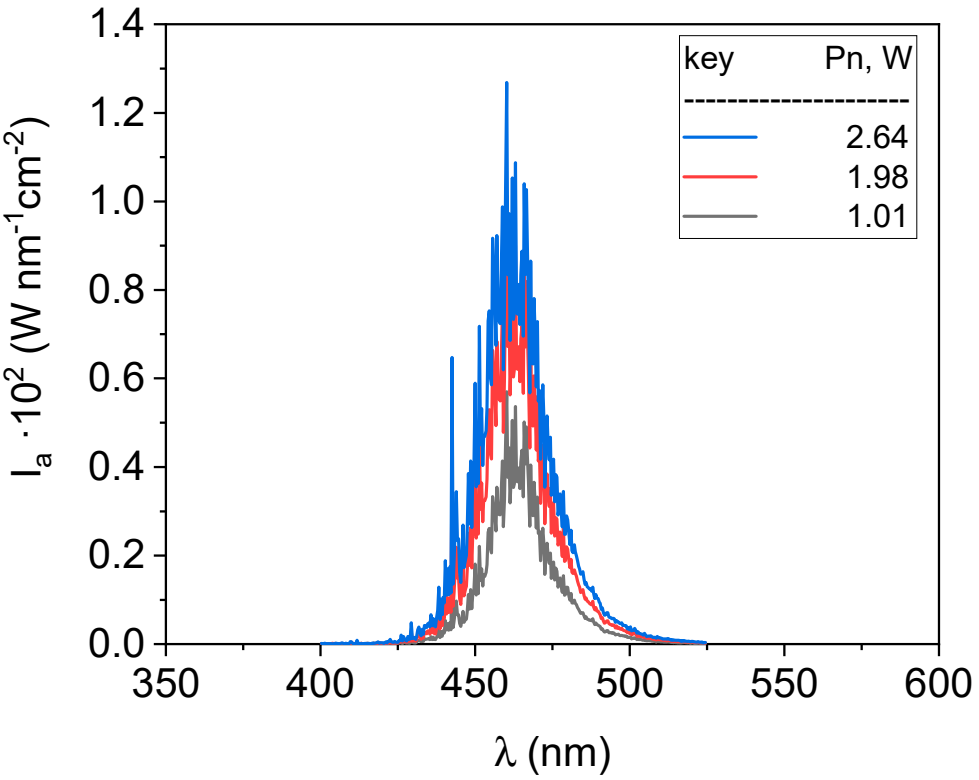

Figure 11. Discretised spectral irradiance measured at the reactor window for different lamp nominal powers (Pn).

Additionally, a study to estimate the light scattering by the solid through the walls of the reactor was accomplished. In addition to the light irradiance at the bottom of the reactor, 0.1, 0.25, and 0.5 g·L^{-1} of goethite was measured. Finally, the flux reflexed by the surface of the reactor window parallel to the light beam was also measured. The points where the scattering out was measured are summarised in Figure S1, and the spectra obtained are plotted in Figures S2 and S3.

3.3. Analytical Methods

The organic compounds concentration in reaction samples were identified and quantified by Gas Chromatography (Agilent 6890N, Santa Clara, CA, USA) with a Mass Spectrometry Detector (GC/MS). The reaction samples were also quantified using a GC (Agilent 6890 gas chromatograph, Santa Clara, CA, USA) with a Flame Ionisation Detector (GC/FID) and an Electron Capture Detector (GC/ECD) simultaneously. Previously, 4 mL of the filtered aqueous phase (once the goethite was removed from the reaction sample and therefore, the reaction evolution was quenched), were extracted with 0.8 mL of n-hexane. The mixture of both phases was shaken for 2 min followed by 10 min of settlement, allowing the organic phase separation by decantation. The analytical methods used in the present work have been reported elsewhere [54]. A chromatography column HP-5MS (30 m × 0.25 mm ID × 0.25 μm) was used as a stationary phase and a constant flow rate of 1.7 mL·min^{-1} of helium was used as a mobile phase. One μL of the liquid sample was injected (injection port temperature: 250 °C). The chromatographic oven worked under a programmed-temperature gradient (starting temperature =80 °C, increasing the temperature at a rate of 18 °C·min^{-1} up to 180 °C, and then keeping it constant for 15 min).

The concentration of H_2O_2 was determined by colorimetric titration, using a spectrophotometer at 410 nm [55] (BOECO S-20 UV-VIS, Hamburg, Germany). The pH was measured with a Basic 20-CRISON pH (Barcelona, Spain) electrode.

Ionic organic by-products, such as carboxylic acids and chlorides, were measured by Ion Chromatography (Metrohm 761 Compact IC, Gallen, Suiza) with anionic chemical suppression and a conductivity detector, using a SUPP5 5-250 column (25 cm length, 4 mm diameter) and an aqueous solution (0.7 $mL \cdot min^{-1}$) of Na_2CO_3 (3.2 mM) and $NaHCO_3$ (1 mM) as mobile phase. The iron content in the aqueous solution was measured by spectroscopy of atomic emission (AES MP-4100 Agilent Technology, Santa Clara, CA, USA) at a wavelength of 259.94 nm and a nebuliser pressure of 100 kPa.

The goethite's transmittance was obtained using a UV-VIS Spectrophotometer (Shimadzu, Kyoto, Japan) coupled with an integrating sphere and an accessory Selection Guide for Solids, measuring the diffuse (and total) transmittance of the solid.

The irradiance and the intensity of the LED lamp were measured using a Flame UV-VIS spectrometer within the wavelength range 200–850 nm coupled with a monacolin UV-Visible optical fiber of 100 µm of core diameter using a cosine corrector (Ocean Insight, Duiven, The Netherlands). The spectrometer and fiber was radiometrically calibrated for use with a cosine corrector (CC-3) using a HL-3P-CAL lamp (Ocean Insight, Duiven, The Netherlands).

3.4. CWPO Experiments

A previous set of experiments was carried at 25 °C and neutral pH to investigate if the reaction could take place in absence of oxidant, catalyst, or light. The experimental conditions of the blank runs (B1 to B5) are summarised in Table S1. They were carried out in the experimental setup shown in Figure 9, and the reactions lasted for 6 h.

The effect of the initial concentration of oxidant (H_2O_2), irradiance, and catalyst concentration (goethite) on the 124-TCB abatement was studied in runs R1 to R12 in Table S1).

The reactor, shown in Figure 9, was initially loaded with 100 mL of synthetic polluted water (28 $mg \cdot L^{-1}$ of 124-TCB). Then, the goethite was added. At this point, the lamp was turned on. The agitation speed was fixed at 350 rpm, avoiding mass transfer limitations. The reaction started when H_2O_2 was added, representing zero time. The runs were carried at neutral initial pH, and the temperature of the reaction mixture was kept at 25 °C.

Reaction samples were analysed at different times. About 4 mL of the reaction media was taken, and the goethite was separated from the aqueous phase using a nylon filter (0.22 µm). The aqueous phase (4 mL) was extracted with 0.8 mL of n-hexane and analysed by GC-MS. The concentrations of 124-TCB and H_2O_2 in the aqueous phase were measured with time. At the end of the reaction time, the chloride ions generated from 124-TCB dechlorination were quantified. Moreover, the Fe (III) leached to the aqueous phase was measured at the end of the reaction time to elucidate if the reaction was heterogeneous or homogeneous. Runs were carried out by triplicate, with the standard deviation being lower than 5% in all cases.

As can be seen in Table S1, the influence of H_2O_2 concentration was investigated in runs R1 to R3 using different doses of hydrogen peroxide in a range of 1–10 times the theoretical stoichiometric amount ($R = C_{H2O2}:C_{H2O2,stq}$), which was calculated for the complete mineralisation of the pollutant (1.8 mM) to carbon dioxide, water, and chloride. The influence of goethite concentration on the pollutant conversion was also investigated in runs R4 to R6, varying it within the range 0.1–1 $g \cdot L^{-1}$. Finally, the power of the LED emitter was tested between 1.04 and 3.13 W.

3.5. Catalyst Stability Test

The catalyst stability was studied in additional runs using the batch well-mixed reactor setup shown in Figure 9. In the first cycle, the reactor was loaded with 0.1 $g \cdot L^{-1}$ of goethite, 100 mL of Milli-Q water, and 18 mg of pure 124-TCB. The amount of hydrogen peroxide added was ten times the stoichiometric required to mineralise the mass of 124-TCB added (18 mM). The 124-TCB added was initially present as an organic phase partially dissolved in the aqueous phase. As the reaction progresses, the 124-TCB in the aqueous phase was

oxidised, and a new equilibrium between the organic and the aqueous phases was reached until the initial mass of 124-TCB added was completely oxidised and disappeared from the reaction medium. This first cycle lasted 24 h. A new cycle begins by adding 18 mg of pure 124-TCB to the reaction medium obtained in the previous cycle without replacing the catalyst. Hydrogen peroxide was measured at the end of the cycle, and the reacted amount was replaced before the starting of the following cycle. This procedure was repeated up to 5 cycles. Each new cycle lasted for 24 h. The reactor content after 1 cycle, 2 cycles, 3 cycles, 4 cycles, and 5 cycles was sacrificed. Chlorides, iron cation, and H_2O_2 concentration were measured in the aqueous phase. Following, 20 mL of n-hexane were added to the total reactor media. The mixture was agitated, and GC/MS was used to analyse the COCs extracted in the organic phase.

4. Conclusions

It was proved that goethite intensified by VIS LED light is an effective system for the CWPO of 124-TCB. This contaminant was selected as a model compound of COC that are commonly found as pollutants in the aqueous phase. It was confirmed that visible monochromatic LED light (470 nm) enhances the 124-TCB abatement. This can be explained because the light lamp, at the selected wavelength attending to the optical properties of goethite, promotes the reduction of Fe (III) in the goethite surface to Fe (II), which yields hydroxyl radicals faster than Fe (III). Moreover, this process can be carried out at neutral pH and room temperature. It was found that the oxidation of 124-TCB (around 90% at the selected conditions: I = 0.24 $W \cdot cm^{-2}$, 10 times the stoichiometric H_2O_2 amount, 0.1 $g \cdot L^{-1}$ of goethite and 6 h) results in its dehalogenation (confirmed by the chloride production), and only short-chain organic acids (mainly acetic acid) were detected as oxidation by-products, meaning that this treatment leads to the detoxification of the polluted water. The photonic efficiencies indicate the energy performance attained with the process and the cost associated with the catalyst load used. A positive effect of hydrogen peroxide concentration, light irradiance on the reaction rate, and an optimal catalyst concentration value (0.1 $g \cdot L^{-1}$) was found. These reactions proved the high stability of goethite, promoting the oxidation of 124-TCB after 120 h of reaction time.

Supplementary Materials: The following are available online at https://www.mdpi.com/2073-4344/11/1/139/s1, Figure S1: Measuring points of the average absolute irradiance using to calculate the scattering out of photons flow. Figure S2: Average absolute irradiance vs. wavelength measured in the point marked in Figure S1 to study the scattering out of the light through the walls of the reactor, L1, L2, and L3 at different values of the incident irradiance and catalyst concentration. Figure S3: Average of absolute irradiance vs. wavelength measured in the point marked in Figure S1 to study the scattering out of the light through the bottom of the reactor (Fb) and the surface of the reaction mixture (Ft). At different values of the incident irradiance and catalyst concentration. Table S1: Experimental conditions of runs carried out to study the effect of the variables on 124-TCB abatement at 25 °C and neutral pH. Table S2: Photonic efficiency calculated using the photons flow irradiated through the reactor window.

Author Contributions: Conceptualisation, D.L. and A.S.; methodology, D.L. and A.S.; investigation, D.L. and A.S.-Y.; resources, A.S.; data curation, L.Ó.C. and C.M.D.; writing—original draft preparation, D.L. and A.S.-Y.; writing—review and editing, L.Ó.C. and C.M.D.; supervision, A.S.; project administration, A.S.; funding acquisition, A.S. All authors have read and agreed to the published version of the manuscript.

Funding: This work was supported by Regional Government of Madrid, project CARESOIL (S2018/EMT-4317), and from the Spanish Ministry of Economy, Industry and Competitiveness, project PID2019-105934RB-I00. This work has also received funding from the European Union's Horizon 2020 research and innovation program under the Marie Skłodowska-Curie Grant Agreement N° 844209 SPFPs.

Conflicts of Interest: The authors declare no conflict of interest.

References

1. Coquery, M.; Morin, A.; Bécue, A.; Lepot, B. Priority substances of the European Water Framework Directive: Analytical challenges in monitoring water quality. *TrAC Trends Anal. Chem.* **2005**, *24*, 117–127. [CrossRef]
2. Schroll, R.; Brahushi, F.; Dörfler, U.; Kühn, S.; Fekete, J.; Munch, J.C. Biomineralisation of 1,2,4-trichlorobenzene in soils by an adapted microbial population. *Environ. Pollut.* **2004**, *127*, 395–401. [CrossRef] [PubMed]
3. Li, J.-H.; Sun, X.-F.; Yao, Z.-T.; Zhao, X.-Y. Remediation of 1,2,3-trichlorobenzene contaminated soil using a combined thermal desorption–molten salt oxidation reactor system. *Chemosphere* **2014**, *97*, 125–129. [CrossRef] [PubMed]
4. Zhang, T.; Li, X.; Min, X.; Fang, T.; Zhang, Z.; Yang, L.; Liu, P. Acute toxicity of chlorobenzenes in Tetrahymena: Estimated by microcalorimetry and mechanism. *Environ. Toxicol. Pharmacol.* **2012**, *33*, 377–385. [CrossRef] [PubMed]
5. Van Wijk, D.; Thompson, R.S.; De Rooij, C.; Garny, V.; Lecloux, A.; Kanne, R. 1,2-Dichlorobenzene marine risk assessment with special reference to the OSPARCOM region: North Sea. *Environ. Monit. Assess.* **2004**, *97*, 87–102. [CrossRef] [PubMed]
6. Van Wijk, D.; Cohet, E.; Gard, A.; Caspers, N.; van Ginkel, C.; Thompson, R.; de Rooij, C.; Garny, V.; Lecloux, A. 1,2,4-Trichlorobenzene marine risk assessment with special emphasis on the Osparcom region North Sea. *Chemosphere* **2006**, *62*, 1294–1310. [CrossRef]
7. Boutonnet, J.C.; Thompson, R.S.; De Rooij, C.; Garny, V.; Lecloux, A.; Van Wijk, D. 1,4-Dichlorobenzene marine risk assessment with special reference to the OSPARCOM region: North Sea. *Environ. Monit. Assess.* **2004**, *97*, 103–117. [CrossRef]
8. Parsons, S. *Advanced Oxidation Processes for Water and Wastewater Treatment*; IWA Publishing: London, UK, 2004.
9. Durkic, T.; Jazic, J.M.; Isakovski, M.K.; Maletic, S.; Tubic, A.; Dalmacija, B.; Agbaba, J. Ultraviolet/Hydrogen Peroxide Oxidative Degradation of 1,2,3-Trichlorobenzene: Influence of Water Matrix and Toxicity Assessment. *Environ. Eng. Sci.* **2019**, *36*, 947–957. [CrossRef]
10. Lhotský, O.; Krákorová, E.; Mašín, P.; Žebrák, R.; Linhartová, L.; Křesinová, Z.; Kašlík, J.; Steinová, J.; Rødsand, T.; Filipová, A.; et al. Pharmaceuticals, benzene, toluene and chlorobenzene removal from contaminated groundwater by combined UV/H2O2 photo-oxidation and aeration. *Water. Res.* **2017**, *120*, 245–255. [CrossRef]
11. Dilmeghani, M.; Zahir, K.O. Kinetics and Mechanism of Chlorobenzene Degradation in Aqueous Samples Using Advanced Oxidation Processes. *J. Environ. Qual.* **2001**, *30*, 2062. [CrossRef]
12. Pagano, M.; Volpe, A.; Lopez, A.; Mascolo, G.; Ciannarella, R. Degradation of chlorobenzene by Fenton-like processes using zero-valent iron in the presence of Fe3+and Cu2+. *Environ. Technol.* **2011**, *32*, 155–165. [CrossRef] [PubMed]
13. Masten, S.J.; Galbraith, M.J.; Davies, S.H.R. Oxidation of 1,3,5-trichlorobenzene using advanced oxidation processes. *Ozone Sci. Eng.* **1997**, *18*, 535–547. [CrossRef]
14. Sedlak, D.L.; Andren, A.W. Oxidation of chlorobenzene with Fenton's reagent. *Environ. Sci. Technol.* **1991**, *25*, 777–782. [CrossRef]
15. Kuang, Y.; Wang, Q.P.; Chen, Z.L.; Megharaj, M.; Naidu, R. Heterogeneous Fenton-like oxidation of monochlorobenzene using green synthesis of iron nanoparticles. *J. Colloid Interface Sci.* **2013**, *410*, 67–73. [CrossRef] [PubMed]
16. Zazou, H.; Oturan, N.; Sonmez-Celebi, M.; Hamdani, M.; Oturan, M.A. Mineralization of chlorobenzene in aqueous medium by anodic oxidation and electro-Fenton processes using Pt or BDD anode and carbon felt cathode. *J. Electroanal. Chem.* **2016**, *774*, 22–30. [CrossRef]
17. Karthikeyan, S.; Boopathy, R.; Gupta, V.K.; Sekaran, G. Preparation, characterizations and its application of heterogeneous Fenton catalyst for the treatment of synthetic phenol solution. *J. Mol. Liq.* **2013**, *177*, 402–408. [CrossRef]
18. Hou, X.J.; Huang, X.P.; Jia, F.L.; Ai, Z.H.; Zhao, J.C.; Zhang, L.Z. Hydroxylamine Promoted Goethite Surface Fenton Degradation of Organic Pollutants. *Environ. Sci. Technol.* **2017**, *51*, 5118–5126. [CrossRef]
19. Neyens, E.; Baeyens, J. A review of classic Fenton's peroxidation as an advanced oxidation technique. *J. Hazard. Mater.* **2003**, *98*, 33–50. [CrossRef]
20. Sreeja, P.H.; Sosamony, K.J. A Comparative Study of Homogeneous and Heterogeneous Photo-fenton Process for Textile Wastewater Treatment. *Procedia Technol.* **2016**, *24*, 217–223. [CrossRef]
21. Munoz, M.; Domínguez, P.; De Pedro, Z.M.; Casas, J.A.; Rodriguez, J.J. Naturally-occurring iron minerals as inexpensive catalysts for CWPO. *Appl. Catal. B-Environ.* **2017**, *203*, 166–173. [CrossRef]
22. Ren, M.; Qian, X.F.; Fang, M.Y.; Yue, D.T.; Zhao, Y.X. Ferric (hydr)oxide/mesoporous carbon composites as Fenton-like catalysts for degradation of phenol. *Res. Chem. Intermediat.* **2018**, *44*, 4103–4117. [CrossRef]
23. Baloyi, J.; Ntho, T.; Moma, J. Synthesis and application of pillared clay heterogeneous catalysts for wastewater treatment: A review. *Rsc Adv.* **2018**, *8*, 5197–5211. [CrossRef]
24. Wang, H.; Jiang, H.; Wang, S.; Shi, W.B.; He, J.C.; Liu, H.; Huang, Y.M. Fe3O4-MWCNT magnetic nanocomposites as efficient peroxidase mimic catalysts in a Fenton-like reaction for water purification without pH limitation. *Rsc Adv.* **2014**, *4*, 45809–45815. [CrossRef]
25. Watts, R.J.; Jones, A.P.; Chen, P.H.; Kenny, A. Mineral-catalyzed Fenton-like oxidation of sorbed chlorobenzenes. Water. *Environ. Res.* **1997**, *69*, 269–275. [CrossRef]
26. Feng, J.; Hu, X.; Yue, P.L.; Zhu, H.Y.; Lu, G.Q. Degradation of azo-dye orange II by a photoassisted Fenton reaction using a novel composite of iron oxide and silicate nanoparticles as a catalyst. *Ind. Eng. Chem. Res.* **2003**, *42*, 2058–2066. [CrossRef]
27. Martínez, F.; Calleja, G.; Melero, J.A.; Molina, R. Heterogeneous photo-Fenton degradation of phenolic aqueous solutions over iron-containing SBA-15 catalyst. *Appl. Catal. B Environ.* **2005**, *60*, 181–190. [CrossRef]

28. Kwan, W.P.; Voelker, B.M. Rates of hydroxyl radical generation and organic compound oxidation in mineral-catalyzed Fenton-like systems. *Environ. Sci. Technol.* **2003**, *37*, 1150–1158. [CrossRef]
29. Lorenzo, D.; Dominguez, C.M.; Romero, A.; Santos, A. Wet Peroxide Oxidation of Chlorobenzenes Catalyzed by Goethite and Promoted by Hydroxylamine. *Catalysts* **2019**, *9*, 553. [CrossRef]
30. Abdelhaleem, A.; Chu, W. Prediction of carbofuran degradation based on the hydroxyl radical's generation using the FeIII impregnated N doped-TiO2/H2O2/visible LED photo-Fenton-like process. *Chem. Eng. J.* **2020**, *382*, 122930. [CrossRef]
31. Clarizia, L.; Russo, D.; Di Somma, I.; Marotta, R.; Andreozzi, R. Homogeneous photo-Fenton processes at near neutral pH: A review. *Appl. Catal. B Environ.* **2017**, *209*, 358–371. [CrossRef]
32. Nitoi, I.; Oncescu, T.; Oancea, P. Mechanism and kinetic study for the degradation of lindane by photo-Fenton process. *J. Ind. Eng. Chem.* **2013**, *19*, 305–309. [CrossRef]
33. Cruz-González, G.; Julcour, C.; Chaumat, H.; Bourdon, V.; Ramon-Portugal, F.; Gaspard, S.; Jáuregui-Haza, U.J.; Delmas, H. Degradation of chlordecone and beta-hexachlorocyclohexane by photolysis, (photo-)fenton oxidation and ozonation. *J. Environ. Sci. Health Part B Pestic. Contam. Agric. Wastes* **2018**, *53*, 121–125. [CrossRef]
34. Evgenidou, E.; Konstantinou, I.; Fytianos, K.; Poulios, I. Oxidation of two organophosphorous insecticides by the photo-assisted Fenton reaction. *Water Res.* **2007**, *41*, 2015–2027. [CrossRef] [PubMed]
35. Ruppert, G.; Bauer, R.; Heisler, G. The photo-Fenton reaction—An effective photochemical wastewater treatment process. *J. Photochem. Photobiol. A Chem.* **1993**, *73*, 75–78. [CrossRef]
36. Amani-Ghadim, A.R.; Alizadeh, S.; Khodam, F.; Rezvani, Z. Synthesis of rod-like α-FeOOH nanoparticles and its photocatalytic activity in degradation of an azo dye: Empirical kinetic model development. *J. Mol. Catal. A-Chem.* **2015**, *408*, 60–68. [CrossRef]
37. Wu, Y.; Hu, W.; Xie, R.; Liu, X.; Yang, D.; Chen, P.; Zhang, J.; Zhang, F. Composite of nano-goethite and natural organic luffa sponge as template: Synergy of high efficiency adsorption and visible-light photocatalysis. *Inorg. Chem. Commun.* **2018**, *98*, 115–119. [CrossRef]
38. Ortiz de la Plata, G.B.; Alfano, O.M.; Cassano, A.E. Decomposition of 2-chlorophenol employing goethite as Fenton catalyst II: Reaction kinetics of the heterogeneous Fenton and photo-Fenton mechanisms. *Appl. Catal. B Environ.* **2010**, *95*, 14–25. [CrossRef]
39. Ortiz de la Plata, G.B.; Alfano, O.M.; Cassano, A.E. Optical properties of goethite catalyst for heterogeneous photo-Fenton reactions: Comparison with a titanium dioxide catalyst. *Chem. Eng. J.* **2008**, *137*, 396–410. [CrossRef]
40. Mameri, Y.; Debbache, N.; Benacherine, M.e.m.; Seraghni, N.; Sehili, T. Heterogeneous photodegradation of paracetamol using Goethite/H 2 O 2 and Goethite/oxalic acid systems under artificial and natural light. *J. Photochem. Photobiol. A Chem.* **2016**, *315*, 129–137. [CrossRef]
41. Benacherine, M.e.m.; Debbache, N.; Ghoul, I.; Mameri, Y. Heterogeneous photoinduced degradation of amoxicillin by Goethite under artificial and natural irradiation. *J. Photochem. Photobiol. A Chem.* **2017**, *335*, 70–77. [CrossRef]
42. Shang, X.; Yang, L.; Ouyang, D.; Zhang, B.; Zhang, W.; Gu, M.; Li, J.; Chen, M.; Huang, L.; Qian, L. Enhanced removal of 1,2,4-trichlorobenzene by modified biochar supported nanoscale zero-valent iron and palladium. *Chemosphere* **2020**, *249*, 126518. [CrossRef] [PubMed]
43. Zhao, Y.; He, P.; Zhang, Y.H.; Ma, S.C. Removal of trichlorobenzene using 'oxygen-enriched' highly active absorbent. *Environ. Technol.* **2011**, *32*, 27–35. [CrossRef] [PubMed]
44. Molina, R.; Segura, Y.; Martínez, F.; Melero, J.A. Immobilization of active and stable goethite coated-films by a dip-coating process and its application for photo-Fenton systems. *Chem. Eng. J.* **2012**, *203*, 212–222. [CrossRef]
45. Wang, Y.; Gao, Y.; Chen, L.; Zhang, H. Goethite as an efficient heterogeneous Fenton catalyst for the degradation of methyl orange. *Catal. Today* **2015**, *252*, 107–112. [CrossRef]
46. Zhang, G.; Wang, Q.; Zhang, W.; Li, T.; Yuan, Y.; Wang, P. Effects of organic acids and initial solution pH on photocatalytic degradation of bisphenol A (BPA) in a photo-Fenton-like process using goethite (α-FeOOH). Photochem. *Photobiol. Sci.* **2016**, *15*, 1046–1053. [CrossRef]
47. Gajović, A.; Silva, A.M.T.; Segundo, R.A.; Šturm, S.; Jančar, B.; Čeh, M. Tailoring the phase composition and morphology of Bi-doped goethite–hematite nanostructures and their catalytic activity in the degradation of an actual pesticide using a photo-Fenton-like process. *Appl. Catal. B Environ.* **2011**, *103*, 351–361. [CrossRef]
48. Barbash, A.M.; Hoag, G.E.; Nadim, F. Oxidation and Removal of 1,2,4-Trichlorobenzene using Sodium Persulfate in a Sorption-Desorption Experiment. *Water Air Soil Pollut.* **2006**, *172*, 67–80. [CrossRef]
49. Lin, S.; Su, G.; Zheng, M.; Jia, M.; Qi, C.; Li, W. The degradation of 1,2,4-trichlorobenzene using synthesized Co3O4 and the hypothesized mechanism. *J. Hazard. Mater.* **2011**, *192*, 1697–1704. [CrossRef]
50. De León, M.A.; Sergio, M.; Bussi, J.; Ortiz De La Plata, G.B.; Alfano, O.M. Heterogeneous photo-Fenton process using iron-modified regional clays as catalysts: Photonic and quantum efficiencies. *Environ. Sci. Pollut. Res.* **2019**, *26*, 12720–12730. [CrossRef]
51. Conte, L.O.; Querini, P.; Albizzati, E.D.; Alfano, O.M. Photonic and quantum efficiencies for the homogeneous photo-Fenton degradation of herbicide 2,4-D using different iron complexes. *J. Chem. Technol. Biotechnol.* **2014**, *89*, 1967–1974. [CrossRef]
52. Munoz, M.; de Pedro, Z.M.; Casas, J.A.; Rodriguez, J.J. Assessment of the generation of chlorinated byproducts upon Fenton-like oxidation of chlorophenols at different conditions. *J. Hazard. Mater.* **2011**, *190*, 993–1000. [CrossRef] [PubMed]
53. Babushok, V.I.; Linstrom, P.J.; Reed, J.J.; Zenkevich, I.G.; Brown, R.L.; Mallard, W.G.; Stein, S.E. Development of a database of gas chromatographic retention properties of organic compounds. *J. Chromatogr. A* **2007**, *1157*, 414–421. [CrossRef] [PubMed]

54. Santos, A.; Fernandez, J.; Guadano, J.; Lorenzo, D.; Romero, A. Chlorinated organic compounds in liquid wastes (DNAPL) from lindane production dumped in landfills in Sabinanigo (Spain). *Environ. Pollut.* **2018**, *242*, 1616–1624. [CrossRef] [PubMed]
55. Eisenberg, G. Colorimetric Determination of Hydrogen Peroxide. *Ind. Eng. Chem. Anal. Ed.* **1943**, *15*, 327–328. [CrossRef]